

Single-Component White-Light Emission in 2D Hybrid Perovskites with Hybridized Halogen Atoms

Guojun Zhou, Mingze Li, Jing Zhao, Maxim S. Molochev, and Zhiguo Xia*

With single-component photoinduced white-light (WL) emission, low-dimensional hybrid halide perovskites have emerged as a new generation of luminescent materials; however, the effect of halogens on the intrinsic light emissions and the corresponding mechanisms is still unknown. Herein, the investigation of a family of two-dimensional (2D) hybrid perovskites $R_2PbBr_{4-x}Cl_x$ ($R = BA^+$, PMA^+ , PEA^+ ; $x = 0, 1, 2, 3, 4$) highlights the influence of halogens on intrinsic emission to reveal the dependence of the photoluminescence on the nature and contribution of the halogens. Ultrabroad emissions covering the entire visible-light region are achieved in the halogen hybrid systems with the stoichiometry of $R_2PbBr_2Cl_2$ ($R = BA^+$, PMA^+ , PEA^+), showing their potential as single-component WL phosphors in solid-state lighting devices. The origin of the WL emissions is the synergistic recombination emission of free excitons and self-trapped excitons. The ratio of halogens (Br/Cl) is confirmed to be a critical factor to fine-tune the intrinsic emission properties. This work provides a feasible strategy to achieve single-component WL emission in 2D hybrid perovskites, and proposes a method for regulating halogen contents for optimizing luminescent properties.

WL can be generated and the possibilities of using these materials for solid-state lighting applications.^[1a,4b,5] In 2014, Karunadasa and co-workers first reported two families of 2D layered perovskites (N -MEDA) $PbBr_{4-x}Cl_x$ (N -MEDA = N^1 -methylethane-1, 2-diammonium, $x = 0-1.2$) and (EDBE) PbX_4 (EDBE = 2, 2'-(ethylenedioxy) bis(ethylammonium), $X = Cl$ and Br), which exhibited stable WL emission and with a relatively high photoluminescence quantum yield (PLQY) of 9% observed in (EDBE) $PbBr_4$.^[4b] Since then, several 2D hybrid perovskites, and some one-dimensional (1D) and zero-dimensional (0D) metal halide hybrids have been demonstrated to exhibit WL emission at room temperature.^[1b,5b,c,6] This broadband emission in low-dimensional metal halides is usually associated with structural deformation in the crystal lattice, which induces the self-trapped excitons


1. Introduction

Hybrid halide perovskites materials have received considerable attention due to their many applications in the fields of light-emitting diodes (LEDs),^[1] solar cells,^[1,c,2] lasers,^[3] etc. Among these materials, low-dimensional metal halides are currently becoming a new focus for solid-state lighting because of their good stability and unique broadband emission.^[4] Most white-light (WL) emitting perovskite materials reported to date are monolayer two-dimensional (2D) hybrid halides, which opens the exciting prospect of understanding how single-component

(STEs) generated from recombination of excited electron-hole pairs through strong electron-phonon coupling.^[4e,6b,7] Recently, 2D layered hybrid perovskites, including $(C_6H_5C_2H_4NH_3)_2PbBr_2Cl_2$,^[8] $(C_6H_5CH_2NH_3)_2PbBr_{4-x}Cl_x$,^[9] and $(CH_3CH_2NH_3)_4Pb_3Br_{10-x}Cl_x$,^[6b] were also found to be WL emitters. These results clarified the effect of halogens on STEs emissions, and it is generally accepted that this effect is strongly correlated to the structural distortion of the perovskite layers in the ground state.^[7c] However, the precise WL emission mechanism in these materials is still under debate because only the role of halogens on STEs was investigated,

G. J. Zhou, M. Z. Li, Prof. J. Zhao, Prof. Z. G. Xia
The Beijing Municipal Key Laboratory
of New Energy Materials and Technologies
School of Materials Sciences and Engineering
University of Science and Technology Beijing
Beijing 100083, P. R. China
E-mail: xiazg@ustb.edu.cn, xiazg@scut.edu.cn

Prof. M. S. Molochev
Laboratory of Crystal Physics
Kirensky Institute of Physics
Federal Research Center KSC SB RAS
Krasnoyarsk 660036, Russia

 The ORCID identification number(s) for the author(s) of this article can be found under <https://doi.org/10.1002/adom.201901335>.

Prof. M. S. Molochev
Department of Engineering Physics and Radioelectronics
Siberian Federal University
Krasnoyarsk 660041, Russia

Prof. M. S. Molochev
Department of Physics
Far Eastern State Transport University
Khabarovsk 680021, Russia

Prof. Z. G. Xia
State Key Laboratory of Luminescent Materials and Devices and
Guangdong Provincial Key Laboratory of Fiber Laser
Materials and Applied Techniques
South China University of Technology
Guangzhou 510641, P. R. China

DOI: 10.1002/adom.201901335

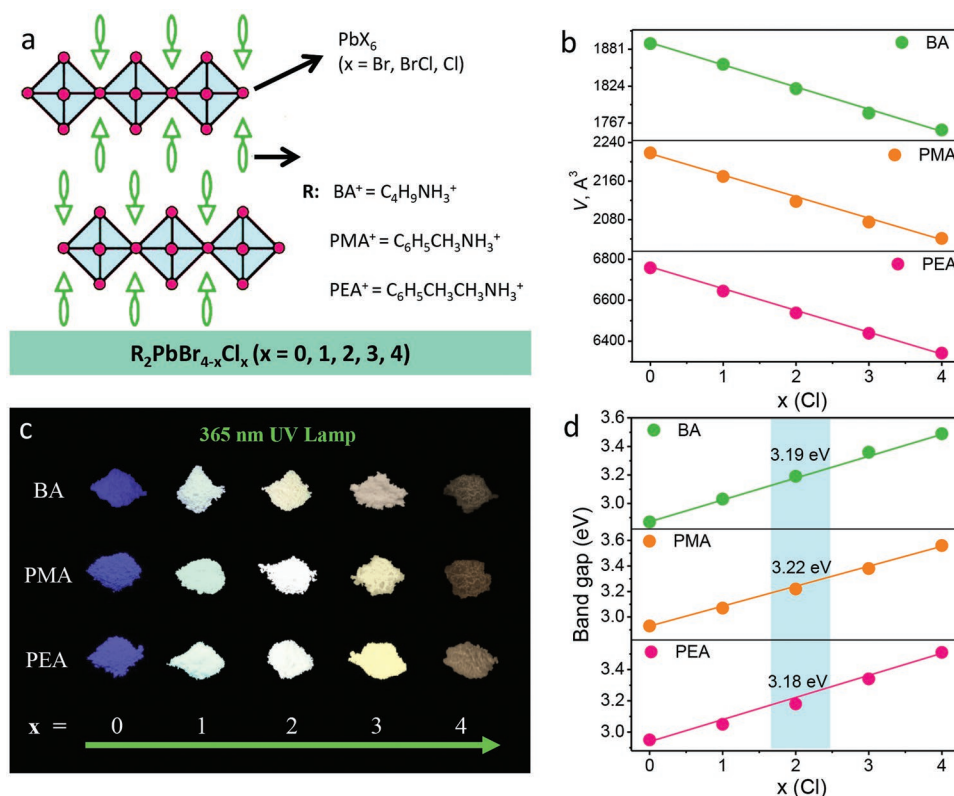


Figure 1. a) The crystal structure of 2D hybrid perovskites with the general formula $R_2PbBr_{4-x}Cl_x$ ($R = BA^+, PMA^+, PEA^+$; $x = 0, 1, 2, 3, 4$). b) The variable trends of the cell volumes of $R_2PbBr_{4-x}Cl_x$ ($R = BA^+, PMA^+, PEA^+$) with different halogen concentrations. c) Luminescent photographs of $R_2PbBr_{4-x}Cl_x$ ($R = BA^+, PMA^+, PEA^+$; $x = 0, 1, 2, 3, 4$) phosphors under a 365 nm UV lamp. d) The variable trends of bandgaps of $R_2PbBr_{4-x}Cl_x$ ($R = BA^+, PMA^+, PEA^+$) phosphors with different halogen concentrations.

while the effect of halogens on free excitons (FEs) and the transmissions between FEs and STEs were ignored.^[5b,7b,10] Thus, it is essential to study the luminescent mechanism to further understand the role of halogens on the intrinsic emissions. Gautier and co-workers reported that the nature of the halogen was an important parameter for tuning the self-trapping depth and the intensity of the resulting broadband emission.^[11] In light of this finding, one can then artificially manipulate the broadband WL emission of 2D halide perovskites by fine-tuning the type and proportion of halogens.

Herein, we introduce a family of 2D hybrid perovskites $R_2PbBr_{4-x}Cl_x$ ($R = BA^+, PMA^+, PEA^+$; $x = 0, 1, 2, 3, 4$) to verify the fundamental relationship between the halogen content and the luminescent properties. The intrinsic light emissions of these compounds showed a strong dependence on the nature and the ratio of the halogens, and a general theory was proposed to explain the broadband emission in 2D hybrid perovskites. Specifically, WL emissions were achieved in the halogen hybrid system $R_2PbBr_2Cl_2$ ($R = BA^+, PMA^+, PEA^+$), showing their potential as single-component WL phosphors for use with ultraviolet light emitting diodes in solid-state lighting devices. Our realizable cases could provide a new understanding of halogen contents on the broadband emission and suggest a feasible strategy to achieve single-component WL emission in 2D hybrid perovskites.

2. Results and Discussion

A series of 2D hybrid perovskites were synthesized by a coprecipitation method with different raw material ratios. Rietveld refinements (Figures S1–S3, Supporting Information) indicate that the as-prepared compounds, $R_2PbBr_{4-x}Cl_x$ ($R = BA^+, PMA^+, PEA^+$; $x = 0, 1, 2, 3, 4$), were of pure phases, and the Br/Cl ratio was taken from the suggested chemical formula and fixed. As shown in Figure 1a, regardless of different organic molecules, each Pb^{2+} ion is coordinated by six Br^- ions, forming octahedra, and these octahedra are linked with each other by nodes forming the 2D layer. Organic ligands are linked with $PbBr_6$ octahedra through hydrogen bonds, $N-H \dots Br$, and cover the 2D layer $(PbBr_6)_n$ from two sides.^[12] Currently, one cannot obtain reliable H-bond parameters because the organic molecules were refined as a rigid bulk, and the refined C, N, H atoms present relatively large ESDs (“Estimated Standard Deviations”).^[13] However, the 2D layered structure type with corner-sharing $Pb(Br,Cl)_6$ octahedra is reliable. In particular, for the different organic ligands of BA, PMA or PEA, the corresponding space groups are $Pbca$, $Cmc2_1$, and $P-1$, respectively. The tuning of halogens only changes the unit cell parameters without influencing their structural assignments. Although there are similar 2D layered types in a series of compounds, $R_2PbBr_{4-x}Cl_x$ ($R = BA^+, PMA^+, PEA^+$; $x = 0, 1, 2, 3, 4$), the local environment of the

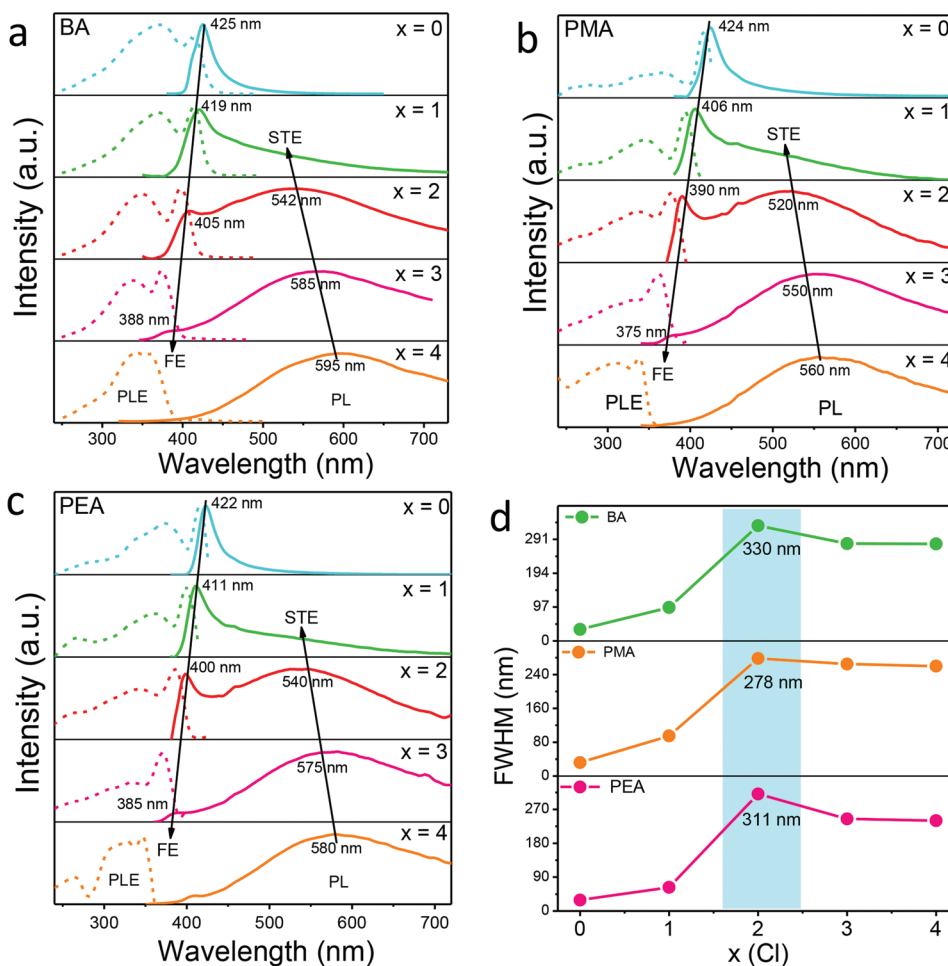


Figure 2. The photoluminescence (PL) and photoluminescence excitation (PLE) spectra of a) $\text{BA}_2\text{PbBr}_{4-x}\text{Cl}_x$, b) $\text{PMA}_2\text{PbBr}_{4-x}\text{Cl}_x$, and c) $\text{PEA}_2\text{PbBr}_{4-x}\text{Cl}_x$ with different halogen ratios; the arrows show variable trends of the narrowband emission of free excitons (FEs) and the broadband emission of self-trapped excitons (STEs). d) The dependence of FWHM values on the halogen contents with the hybrid systems of $\text{R}_2\text{PbBr}_2\text{Cl}_2$ ($\text{R} = \text{BA}^+$, PMA^+ , PEA^+) showing the maximum values of 330, 278, and 311 nm, respectively.

PbX_6 octahedra is affected by various bond lengths and bond angles. The main parameters of processing and refinement of $\text{R}_2\text{PbBr}_{4-x}\text{Cl}_x$ ($\text{R} = \text{BA}^+$, PMA^+ , PEA^+ ; $x = 0, 1, 2, 3, 4$) are listed in Table S1 (Supporting Information). The corresponding cell volumes $V(x)$ decrease with increasing $\text{Cl}(x)$ concentration (Figure 1b), which is in good agreement with the fact that the Cl ion radius (1.81 Å) is smaller than Br ion radius (1.96 Å).^[14] The refinements prove that the suggested chemical formulas are close to the real ratio of raw materials.

As shown in Figure 1c, the luminescence characteristics of $\text{R}_2\text{PbBr}_{4-x}\text{Cl}_x$ ($\text{R} = \text{BA}^+$, PMA^+ , PEA^+ ; $x = 0, 1, 2, 3, 4$) can be visualized under a 365 nm UV lamp, which clearly shows the variation trend of emission when Br ions are gradually substituted by Cl ions. Interestingly, all the abovementioned 2D halogen hybrid perovskites can emit white light, especially in the intermediate composition with $x = 2$. To further evaluate the luminescent properties after halogen ion exchange, diffuse reflectance data were obtained (Figure S4, Supporting Information), and the corresponding bandgap values showed an increasing trend with the increase of Cl ions, as shown in Figure 1d. The results indicate the relative energy levels before

and after halogen exchange for these 2D halogen hybrid perovskites, which can be used to analyze the recombination of FEs.

Figure 2a–c shows the normalized excitation and emission spectra of $\text{BA}_2\text{PbBr}_{4-x}\text{Cl}_x$ ($x = 0, 1, 2, 3, 4$), $\text{PMA}_2\text{PbBr}_{4-x}\text{Cl}_x$ ($x = 0, 1, 2, 3, 4$), and $\text{PEA}_2\text{PbBr}_{4-x}\text{Cl}_x$ ($x = 0, 1, 2, 3, 4$), respectively. As expected, as the Cl concentration (x) increases, all the emission spectra gradually change from a narrow band to ultra-broad dual band, consisting of a narrow peak and a broad peak, and eventually only show one broadband emission. Specifically, the photoluminescence spectra of $\text{R}_2\text{PbBr}_2\text{Cl}_2$ ($\text{R} = \text{BA}^+$, PMA^+ , PEA^+) at room temperature show broadband emissions at ≈ 540 nm and a shoulder at ≈ 400 nm, and the narrow peaks have small Stokes shifts while the broad peaks have large Stokes shifts,^[1b,15] which indicates that the narrowband emission can be attributed to the recombination of FEs, and the broadband emission is due to the recombination of STEs. To further clarify the origin of the broadband emission, a power density dependent emission measurement was performed. As shown in Figure 3, the intensity of the broadband peaks of $\text{R}_2\text{PbBr}_2\text{Cl}_2$ ($\text{R} = \text{BA}^+$, PMA^+ , PEA^+) increases linearly with increasing excitation power and does not reach saturation;^[16] thus we assigned

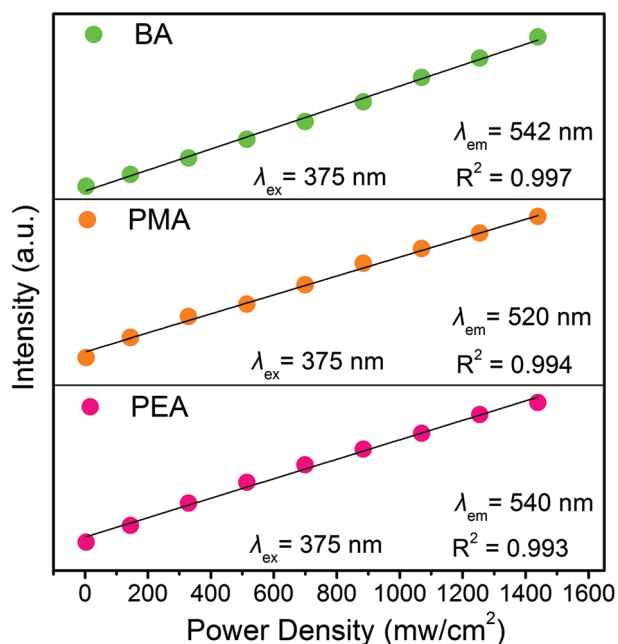


Figure 3. Variation of the emission intensities at 542, 520, and 540 nm excited at 375 nm as a function of the excitation power density of $\text{BA}_2\text{PbBr}_2\text{Cl}_2$, $\text{PMA}_2\text{PbBr}_2\text{Cl}_2$, and $\text{PEA}_2\text{PbBr}_2\text{Cl}_2$.

this broadband as STEs emission. Based on the above discussions, it can be concluded that the hybridization of the halogen component not only regulates the free exciton emissions but also induces the broadband emission from the STEs.

As is well known, the high distortion level of the local octahedral environments implies a more malleable structure, which is more susceptible to generating STEs states upon photoexcitation, thus producing the broadband emission of STEs.^[1b,9,10,11] For 2D hybrid perovskite systems, the overall broadness of the PL emission is heavily influenced by the structural distortion, which is evaluated here by the distortion level of the PbX_6 ($X = \text{Br}, \text{Cl}$) octahedra. The distortions of the octahedra were calculated by the following formula:

$$\Delta d = \left(\frac{1}{6}\right) \sum \left[\frac{d_n - d}{d}\right]^2$$

where d is the average bond length and d_n is the individual Pb-Br/Cl bond length.^[5b] The distortion indexes of $\text{R}_2\text{PbBr}_{4-x}\text{Cl}_x$ ($R = \text{BA}^+, \text{PMA}^+, x = 0, 1, 2, 3, 4$) are shown in Figure S5 (Supporting Information); the halogen hybrid systems with $x = 2$ showed relatively high values, which would favor the resulting extrinsic STEs. In particular, the distortion level is related to the width of the PL emission; the larger the distortion, the broader the width of the PL emission.^[6c] Meanwhile, the dependence of full-width at half-maximum (FWHM) values on the halogen contents is shown in Figure 2d, and the maximum values of the $\text{R}_2\text{PbBr}_2\text{Cl}_2$ ($R = \text{BA}^+, \text{PMA}^+, \text{PEA}^+$) systems are 330, 278, and 311 nm, respectively. It is obvious that the broadband emission of $\text{R}_2\text{PbBr}_2\text{Cl}_2$ ($R = \text{BA}^+, \text{PMA}^+, \text{PEA}^+$) originates from the combined effect of FEs and STEs. To further evaluate the luminescent performance of this series of compounds, the PLQYs are measured at room temperature, as listed in Table 1. The PLQYs of $\text{R}_2\text{PbBr}_2\text{Cl}_2$ ($R = \text{BA}^+, \text{PMA}^+, \text{PEA}^+$) phosphors are 2.03%, 4.21%,

Table 1. The photoluminescence quantum yields (PLQYs) of $\text{R}_2\text{PbBr}_{4-x}\text{Cl}_x$ ($R = \text{BA}^+, \text{PMA}^+, \text{PEA}^+; x = 0, 1, 2, 3, 4$).

PLQY [%]	$x = 0$	$x = 1$	$x = 2$	$x = 3$	$x = 4$
BA	9.4	6.43	2.03	0.99	0.63
PMA	7.35	5.25	4.21	0.63	2.39
PEA	12.56	11.68	6.28	2.86	1.56

6.28%, respectively. As Br ions are gradually substituted by Cl ions, the PLQY values show a tendency to decrease, indicating that the quantum yield of STEs is lower than that of FEs.

As a powerful piece of evidence to reveal the emission mechanisms of FEs and STEs, we performed variable-temperature experiments with $\text{R}_2\text{PbBr}_2\text{Cl}_2$ ($R = \text{BA}^+, \text{PMA}^+, \text{PEA}^+$) from 80 to 300 K, as shown in Figure S6 (Supporting Information). With decreasing temperature, the emission intensity of FEs increases due to the weakening of nonradiative transition at low temperature. Usually, at sufficiently low temperature, the FEs emissions should be dominant compared to those of STEs. Here, we find that the STEs emissions of $\text{R}_2\text{PbBr}_2\text{Cl}_2$ ($R = \text{PMA}^+, \text{PEA}^+$) still dominate the overall emission, suggesting that the activation energy of STEs is affected by the type of organic ligands.^[6c,11a] Importantly, the trend of temperature dependence can be generally summarized as the FWHM of broadband emissions gradually decreasing as the temperature decreases, represented by $\text{PMA}_2\text{PbBr}_2\text{Cl}_2$ (Figure S7, Supporting Information). This phenomenon can be explained by the deactivation of STE emission due to weak electron–phonon coupling at low temperature.^[6c,11a] It is obvious that there is a competitive relationship between FEs and STEs emissions in 2D halide perovskites. To further understand the luminescent mechanism, the decay curves of $\text{R}_2\text{PbBr}_2\text{Cl}_2$ ($R = \text{BA}^+, \text{PMA}^+, \text{PEA}^+$) were measured at different monitoring wavelengths. As illustrated in Figure 4a–c, the PL decay curves monitored at $\lambda_{\text{em}} = 380$ and 390 nm are fitted by a double exponential decay process with $I = A_1 \exp(-t/\tau_1) + A_2 \exp(-t/\tau_2)$, and the average lifetimes can be obtained by using the calculation formula $\tau = (A_1 \tau_1^2 + A_2 \tau_2^2) / (A_1 \tau_1 + A_2 \tau_2)$ with the lifetime values of 0.72 and 2.91 ns for the 380 and 390 nm emission, respectively.^[17] It is noteworthy that the decay curves of $\text{R}_2\text{PbBr}_2\text{Cl}_2$ ($R = \text{BA}^+, \text{PMA}^+, \text{PEA}^+$) monitored at the peaks of 542, 520, and 540 nm, respectively, tend to become single exponential function ($I = I_0 + A \exp(-t/\tau)$). It is inferred that there is one form of radiation transition with relatively long lifetimes of 5.21, 9.51, and 12.56 ns for $\text{R}_2\text{PbBr}_2\text{Cl}_2$ with R representing $\text{BA}^+, \text{PMA}^+, \text{PEA}^+$, respectively, attributing to the recombination of STEs. As described above, the lifetime at the monitoring wavelength of 380 nm is significantly shorter than that of 390 nm. Thus we believe that the lifetime measured at 380 nm is the real lifetime of FEs recombination, while the lifetime at 390 nm is ascribed to the superposition of FEs and STEs. This result also indicates that the broadband emissions of $\text{R}_2\text{PbBr}_2\text{Cl}_2$ ($R = \text{BA}^+, \text{PMA}^+, \text{PEA}^+$) are produced by the combined effect of FEs and STEs. To further reveal the luminescent mechanism of the hybrid intermediate systems, the dependence of the lifetimes of d) $\text{BA}_2\text{PbBr}_2\text{Cl}_2$, e) $\text{PMA}_2\text{PbBr}_2\text{Cl}_2$, and f) $\text{PEA}_2\text{PbBr}_2\text{Cl}_2$ on the emission wavelengths were explored in detail (Figure 4d–f). The lifetime values at the broadband emission attributed to the STEs are close and continuous;

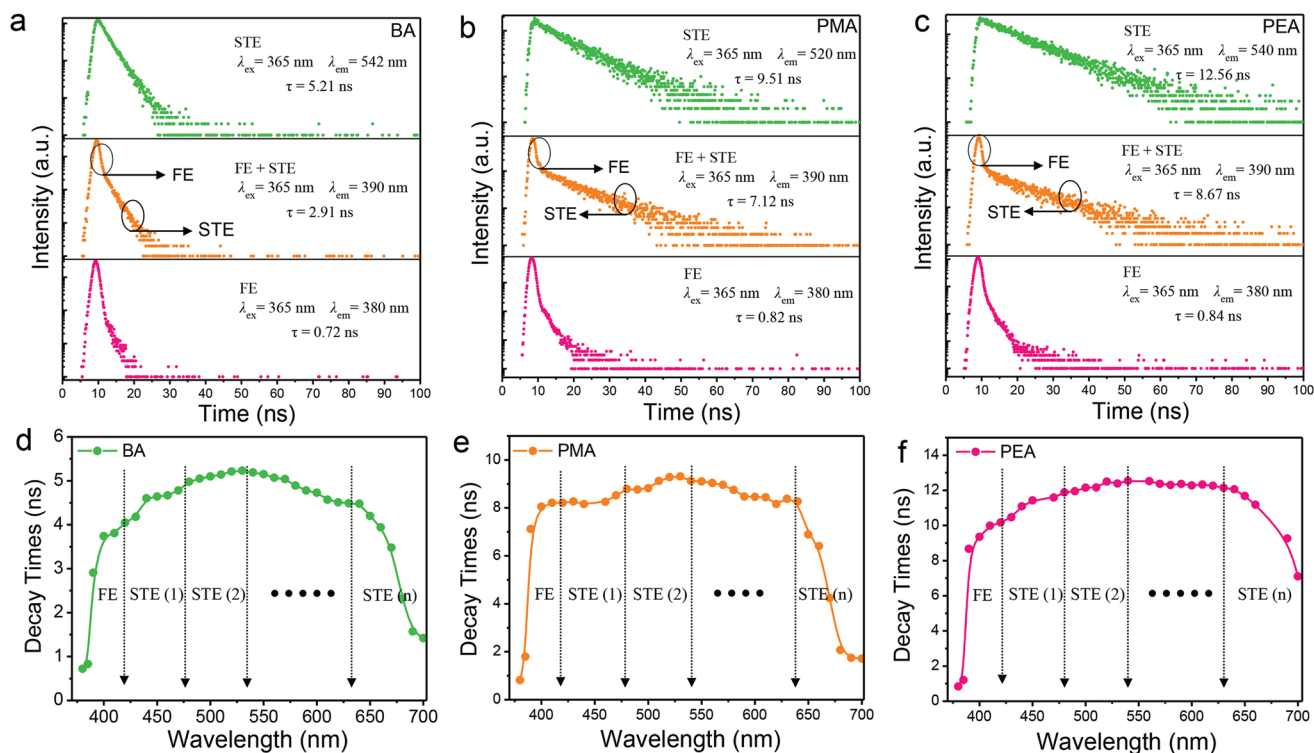


Figure 4. The photoluminescent decay curves of a) $\text{BA}_2\text{PbBr}_2\text{Cl}_2$, b) $\text{PMA}_2\text{PbBr}_2\text{Cl}_2$, and c) $\text{PEA}_2\text{PbBr}_2\text{Cl}_2$ under 365 nm excitation. The dependence of the lifetimes of d) $\text{BA}_2\text{PbBr}_2\text{Cl}_2$, e) $\text{PMA}_2\text{PbBr}_2\text{Cl}_2$, and f) $\text{PEA}_2\text{PbBr}_2\text{Cl}_2$ on the variation of monitoring emission wavelengths.

thus, we propose that there are many self-trapped energy levels, which is the fundamental reason for inducing broadband emission of STEs. Based on that observation, we provide a schematic diagram of the luminescent mechanism of the 2D hybrid perovskites, as shown in Figure 5a–c.^[7b,c] According to the effect of halogens on the energy levels of FEs rather than STEs,^[11a] the energy level of FEs move toward the direction of higher energy due to the increasing trend of bandgaps with the increase of Cl ions. Specifically, in the end member for the Br_4 system with a relatively small bandgap, the lower energy level position allows the excited electrons to recombine as free excitons, so that one can only observe narrowband emissions originating from the

FEs. For the hybrid Br_2Cl_2 system, the levels of FEs and STEs are close to each other; this proximity achieves dual emission due to the balance of energy transfer, resulting in broadband WL emission covering the entire visible-light region. In contrast, in the end member for the Cl_4 system, the high level of the free excitons allows most of the energy to be transferred to the STEs, which causes single broadband emissions of STEs, as observed. However, in general, the luminescent efficiency of STEs in the Cl_4 systems is low, which limits their application as a potential candidate for a single-component white-light emitter. The above results reveal that the broadband WL emission covering the entire visible-light region can be achieved in

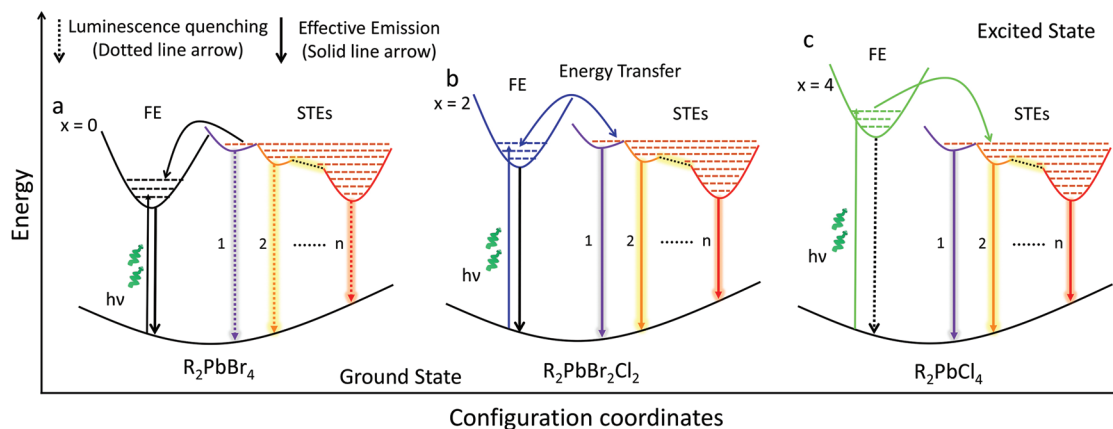


Figure 5. Schematic luminescence mechanism of 2D hybrid perovskites with the recombinations of free excitons and self-trapped excitons: a) R_2PbBr_4 ; b) $\text{R}_2\text{PbBr}_2\text{Cl}_2$; c) R_2PbCl_4 .

the halogen hybrid systems $R_2PbBr_2Cl_2$ ($R = BA^+, PMA^+, PEA^+$). Thus these systems are promising as single-component white-light phosphors for use with ultraviolet lightemitting diodes in solid-state lighting devices.

3. Conclusion

In summary, we have demonstrated a general strategy and synthesized a series of hybrid perovskites compounds, $R_2PbBr_{4-x}Cl_x$ ($R = BA^+, PMA^+, PEA^+$; $x = 0, 1, 2, 3, 4$), with the same 2D layered structures. The nature and proportion of the halogens were verified to be key parameters for tuning the energy levels of the FEs and STEs. Broadband emissions covering the entire visible-light region were obtained in the halogen hybrid system, $R_2PbBr_2Cl_2$ ($R = BA^+, PMA^+, PEA^+$), which originate from the synergistic effects of the recombination emission of FEs and STEs. Meanwhile, this work demonstrates that fine-tuning the halogen content in 2D hybrid perovskites is a facile way to achieve single-component WL emission. Our case study provides a feasible strategy for rationally designing single-component WL phosphors in hybrid luminescent metal halides that are suitable for solid state lighting.

4. Experimental Section

Materials and Preparation: $PbCl_2$, $PbBr_2$ (99.9%, Aladdin), $C_4H_9NH_3Cl$, and $C_4H_9NH_3Br$ (butylamine hydrochloride (BACl), butylamine hydrobromide (BABr), 99.9%, Xi'an p-OLED), $C_6H_5CH_2NH_3Cl$ and $C_6H_5CH_2NH_3Br$ (benzylamine hydrochloride (PMACl), benzylamine hydrobromide (PMABr), 99.9%, Xi'an p-OLED), $C_6H_5CH_2CH_2NH_3Cl$ and $C_6H_5CH_2CH_2NH_3Br$ (2-phenylethanamine hydrochloride (PEACl), 2-phenylethanamine hydrobromide (PEABr), 99.9%, Xi'an p-OLED), C_7H_8 (toluene 99.5%, Sinopharm), and $C_4H_{10}O$ (ethyl ether 99.7%, Sinopharm), N,N' -dimethylformamide (DMF, 99.5%, Aladdin) were all used as received.

The compounds $R_2PbBr_{4-x}Cl_x$ ($R = BA^+, PMA^+, PEA^+$; $x = 0, 1, 2, 3, 4$) were synthesized by a solution coprecipitation method. The precursors BACl/BABr, PMACl/PMABr, PEACl/PEABr (2 mmol) and $PbCl_2/PbBr_2$ (1 mmol) were dissolved in 2 mL of DMF and heated to 90 °C. Toluene was added to the hot clear solution until the solution began to become cloudy. The products $R_2PbBr_{4-x}Cl_x$ ($R = BA^+, PMA^+, PEA^+$; $x = 0, 1, 2, 3, 4$) were thus obtained and washed repeatedly with ethyl ether. After filtration, the precursors were dried at 60 °C for 24 h in a vacuum oven. Halogen hybrids were obtained by adjusting the proportions of precursors and lead halide.

Characterization: The powder diffraction data of $R_2PbBr_{4-x}Cl_x$ ($R = BA^+, PMA^+, PEA^+$; $x = 0, 1, 2, 3, 4$) for Rietveld analysis were collected at room temperature with an AERIS X-ray diffractometer (Cu K α radiation). The step size of 2θ was 0.013°, and the counting time was 5 s per step. The Rietveld refinements were performed using TOPAS 4.2. The PL spectra, photoluminescence excitation (PLE) spectra, luminescence decay curves, and PLQYs were measured by a FLSP9200 fluorescence spectrophotometer (Edinburgh Instruments Ltd., UK). The diffuse reflectance spectra were collected by the Hitachi UH4150 US-vis-near-infrared spectrophotometer using white $BaSO_4$ for calibration. The power-dependent photoluminescence spectra were measured using the 375 nm (LE-LS-375-140TFCA, 1–140 mW).

Supporting Information

Supporting Information is available from the Wiley Online Library or from the author.

Acknowledgements

G.J.Z. and M.Z.L. contributed equally to this work. The present work was supported by the National Natural Science Foundations of China (Grant Nos. 51722202 and 51972118), the Fundamental Research Funds for the Central Universities (D2190980), and the Guangdong Provincial Science & Technology Project (No. 2018A050506004).

Conflict of Interest

The authors declare no conflict of interest.

Keywords

2D halide perovskites, photoluminescence, white-light emission

Received: August 6, 2019

Revised: September 15, 2019

Published online: October 22, 2019

- [1] a) Y. Tian, C. K. Zhou, M. Worku, X. Wang, Y. C. Ling, H. W. Gao, Y. Zhou, Y. Miao, J. J. Guan, B. W. Ma, *Adv. Mater.* **2018**, *30*, 1707093; b) M. D. Smith, B. A. Connor, H. I. Karunadasa, *Chem. Rev.* **2019**, *119*, 3104; c) P. Chen, Y. Bai, M. Q. Lyu, J. H. Yun, M. M. Hao, L. Z. Wang, *Sol. RRL* **2018**, *2*, 1700186; d) S. Adjokatse, H. H. Fang, M. A. Loi, *Mater. Today* **2017**, *20*, 413.
- [2] a) D. H. Cao, C. C. Stoumpos, O. K. Farha, J. T. Hupp, M. G. Kanatzidis, *J. Am. Chem. Soc.* **2015**, *137*, 7843; b) W. Fu, J. Wang, L. Zuo, K. Gao, F. Liu, D. S. Ginger, A. K. Y. Jen, *ACS Energy Lett.* **2018**, *3*, 2086.
- [3] Q. Zhang, R. Su, W. N. Du, X. F. Liu, L. Y. Zhao, S. T. Ha, Q. H. Xiong, *Small Methods* **2017**, *1*, 1700163.
- [4] a) M. I. Saidaminov, O. F. Mohammed, O. M. Bakr, *ACS Energy Lett.* **2017**, *2*, 889; b) E. R. Dohner, A. Jaffe, L. R. Bradshaw, H. I. Karunadasa, *J. Am. Chem. Soc.* **2014**, *136*, 13154; c) Z. W. Xiao, Z. N. Song, Y. F. Yan, *Adv. Mater.* **2019**, 1803792; d) G. H. Wu, C. K. Zhou, W. M. Ming, D. Han, S. Y. Chen, D. Yang, T. Besara, J. Neu, T. Siegrist, M. H. Du, B. W. Ma, A. Dong, *ACS Energy Lett.* **2018**, *3*, 1443; e) C. K. Zhou, H. Lin, S. Lee, M. Chaaban, B. W. Ma, *Mater. Res. Lett.* **2018**, *6*, 552.
- [5] a) E. R. Dohner, E. T. Hoke, H. I. Karunadasa, *J. Am. Chem. Soc.* **2014**, *136*, 1718; b) L. L. Mao, Y. Wu, C. C. Stoumpos, M. R. Wasielewski, M. G. Kanatzidis, *J. Am. Chem. Soc.* **2017**, *139*, 5210; c) H. W. Hu, F. Meier, D. M. Zhao, Y. Abe, Y. Gao, B. B. Chen, T. Salim, E. E. M. Chia, X. F. Qiao, C. Deibel, Y. M. Lam, *Adv. Mater.* **2018**, *30*, 1707621; d) L. T. Dou, A. B. Wong, Y. Yu, M. L. Lai, N. Kornienko, S. W. Eaton, A. Fu, C. G. Bischak, J. Ma, T. Ding, N. S. Ginsberg, L. W. Wang, A. P. Alivisatos, P. D. Yang, *Science* **2015**, *349*, 1518.
- [6] a) Z. Yuan, C. K. Zhou, J. Messier, Y. Tian, Y. Shu, J. M. Wang, Y. Xin, B. W. Ma, *Adv. Opt. Mater.* **2016**, *4*, 2009; b) L. L. Mao, Y. L. Wu, C. C. Stoumpos, B. Traore, C. Katan, J. Even, M. R. Wasielewski, M. G. Kanatzidis, *J. Am. Chem. Soc.* **2017**, *139*, 11956; c) L. L. Mao, P. J. Guo, M. Kepenekian, I. Hadar, C. Katan, J. Even, R. D. Schaller, C. C. Stoumpos, M. G. Kanatzidis, *J. Am. Chem. Soc.* **2018**, *140*, 13078; d) Z. Y. Wu, C. M. Ji, Z. H. Sun, S. S. Wang, S. G. Zhao, W. C. Zhang, L. N. Li, J. H. Luo, *J. Mater. Chem. C* **2018**, *6*, 1171.
- [7] a) X. T. Li, P. J. Guo, M. Kepenekian, I. Hadar, C. Katan, J. Even, C. C. Stoumpos, R. D. Schaller, M. G. Kanatzidis, *Chem.*

- Mater.* **2019**, *31*, 3582; b) T. Hu, M. D. Smith, E. R. Dohner, M. J. Sher, X. Wu, M. T. Trinh, A. Fisher, J. Corbett, X. Y. Zhu, H. I. Karunadasa, A. M. Lindenberg, *J. Phys. Chem. Lett.* **2016**, *7*, 2258; c) M. D. Smith, H. I. Karunadasa, *Acc. Chem. Res.* **2018**, *51*, 619.
- [8] a) S. Yang, Z. Lin, J. Wang, Y. Chen, Z. Liu, E. Yang, J. Zhang, Q. Ling, *ACS Appl. Mater. Interfaces* **2018**, *10*, 15980; b) P. Q. Cai, X. F. Wang, H. J. Seo, X. H. Yan, *Appl. Phys. Lett.* **2018**, *112*, 153901.
- [9] M. H. Jung, *Inorg. Chem.* **2019**, *58*, 6748.
- [10] M. D. Smith, A. Jaffe, E. R. Dohner, A. M. Lindenberg, H. I. Karunadasa, *Chem. Sci.* **2017**, *8*, 4497.
- [11] a) R. Gautier, M. Paris, F. Massuyeau, *J. Am. Chem. Soc.* **2019**, *141*, 12619; b) R. Gautier, F. Massuyeau, G. Galnon, M. Paris, *Adv. Mater.* **2019**, *31*, 1807383.
- [12] D. B. Mitzi, S. Wang, C. A. Feild, C. A. Chess, A. M. Guloy, *Science* **1995**, *267*, 1473.
- [13] H. G. Scott, *J. Appl. Crystallogr.* **1983**, *16*, 159.
- [14] R. D. Shannon, *Acta Crystallogr. A* **1976**, *32*, 751.
- [15] M. D. Smith, B. L. Watson, R. H. Dauskardt, H. I. Karunadasa, *Chem. Mater.* **2017**, *29*, 7083.
- [16] T. Schmidt, K. Lischka, *Phys. Rev. B* **1992**, *45*, 8989.
- [17] C. H. Huang, T. M. Chen, W. R. Liu, Y. C. Chiu, Y. T. Yeh, S. M. Jang, *ACS Appl. Mater. Interfaces* **2010**, *2*, 259.